HHS Public Access

Author manuscript

Int J Hyperthermia. Author manuscript; available in PMC 2016 January 05.

Published in final edited form as:

Int J Hyperthermia. 2015 December ; 31(8): 813–822. doi:10.3109/02656736.2015.1094833.

Localised hyperthermia in rodent models using an MRI-compatible high-intensity focused ultrasound system

Chenchen Bing[1], **Joris Nofiele**[1], **Robert Staruch**[1,2], **Michelle Ladouceur-Wodzak**[1], **Yonatan Chatzinoff**[3], **Ashish Ranjan**[4], and **Rajiv Chopra**[1,5]

[1]Department of Radiology, University of Texas Southwestern Medical Center, Dallas, Texas

[2]Clinical Sites Research Program, Philips Research, Briarcliff Manor, New York

[3]Applied Research Center, University of Texas at Dallas, Dallas, Texas

[4]Center of Veterinary Health Sciences, Oklahoma State University, Stillwater, Oklahoma, USA

[5]Advanced Imaging Research Center, University of Texas Southwestern Medical Center, Dallas, Texas

Abstract

Purpose—Localised hyperthermia in rodent studies is challenging due to the small target size. This study describes the development and characterisation of an MRI-compatible high-intensity focused ultrasound (HIFU) system to perform localised mild hyperthermia treatments in rodent models.

Material and methods—The hyperthermia platform consisted of an MRI-compatible small animal HIFU system, focused transducers with sector-vortex lenses, a custom-made receive coil, and means to maintain systemic temperatures of rodents. The system was integrated into a 3T MR imager. Control software was developed to acquire images, process temperature maps, and adjust output power using a proportional-integral-derivative feedback control algorithm. Hyperthermia exposures were performed in tissue-mimicking phantoms and in a rodent model (n = 9). During heating, an ROI was assigned in the heated region for temperature control and the target temperature was 42 °C; 30 min mild hyperthermia treatment followed by a 10-min cooling procedure was performed on each animal.

Results—3D-printed sector-vortex lenses were successful at creating annular focal regions which enables customisation of the heating volume. Localised mild hyperthermia performed in rats produced a mean ROI temperature of 42.1 ± 0.3 °C. The T10 and T90 percentiles were 43.2 ± 0.4 °C and 41.0 ± 0.3 °C, respectively. For a 30-min treatment, the mean time duration between 41–45 °C was 31.1 min within the ROI.

Correspondence: Rajiv Chopra, PhD, Clements Advanced Medical Imaging Building, Room NE6.252, 2201 Inwood Road, Dallas, TX, 75390, USA. Tel: 214-648-7745. Rajiv.Chopra@UTSouthwestern.edu.

Declaration of interest

The other authors report no conflicts of interest.

Conclusions—The MRI-compatible HIFU system was successfully adapted to perform localised mild hyperthermia treatment in rodent models. A target temperature of 42 °C was well-maintained in a rat thigh model for 30 min.

Keywords

Heat-targeted drug delivery; mild hyperthermia; MR-HIFU; nanoparticles; non-invasive thermometry

Introduction

The therapeutic effects of sustained mild hyperthermia have been documented for decades across a wide range of applications including radio-sensitisation, chemo-sensitisation, and targeted drug delivery [1,2]. Clinically, hyperthermia has been delivered using external and/or interstitial heating applicators employing a range of energy modalities [3,4]. Monitoring of temperatures during hyperthermia has most commonly been achieved with invasive temperature sensors [5], and more recently with magnetic resonance imaging (MRI) [6]. As early as the mid 1980s it was confirmed that significant cell killing could occur when the tissues were heated to >42 °C for longer duration [7,8]. However, in the clinic, achieving reliable heating in the target range of 41–43 °C for extended periods of time has been a significant technical challenge due to the involving of patient physiology and the difficulties of treatment monitoring in deep tissue [9].

For preclinical investigations of mild hyperthermia in small animals there are equally challenging issues to overcome in order to achieve well-controlled spatial and temporal heating. The target volumes are often small (several mm^3), which requires precise localisation of energy. Maintaining the core temperature of animals over the duration of a hyperthermia experiment is difficult, but critical to avoid effects related to systemic hypothermia or hyperthermia [10]. Elevation of core body temperature can often arise because the tumour volume relative to the animal's body weight is a much higher fraction than encountered in humans. An important requirement for achieving a successful localised mild hyperthermia treatment is accurate temperature monitoring of the target volume as well as the animal's core temperature throughout treatment. Finally, it is desirable to have some form of adaptive control of output energy to compensate for changes in the temperature distribution arising from physiological or other sources.

A number of small animal hyperthermia systems have been described in prior academic studies. The most commonly used technique for mild hyperthermia is immersion of the target body part (i.e. leg) in a temperature-controlled water bath [11–14]. This is the simplest approach to implement but suffers from poor localisation and non-uniform heating since the approach relies on thermal conduction from the skin surface. Radiofrequency (RF) and microwave devices have also been used for small animal hyperthermia studies [15–22]. In RF hyperthermia treatments the target tissue is capacitively coupled with multiple applicators connected to an RF generator. For microwave hyperthermia systems, heating is generated using a temperature-controlled microwave ring radiator. Recently, focused ultrasound systems have been developed to perform hyperthermia treatment in small animals

[23–35]. High-intensity focused ultrasound (HIFU) systems are well suited for small animal heating due to the ability to concentrate acoustic energy into a focal volume within a few millimetres. These systems have been integrated with MRI, PET, or ultrasound imaging for image-guided exposures [28,36–39]. When integrated with MRI, MR thermometry can be utilised to monitor and control localised heating. The target temperature can be well maintained for an extended duration (up to 1 h) required for a mild hyperthermia treatment.

The goal of this study was to extend the functionality of an existing preclinical HIFU system to perform sustained mild hyperthermia treatments in rodent models. This study builds upon prior characterisation of the system for ablation and transcranial exposures [40–43]. The HIFU system was integrated with a software platform enabling rapid transfer of images from a 3T MRI scanner to the system for temperature feedback control. Acoustic sector-vortex lenses were designed and used to distribute ultrasound energy across a relevant volume representative of a tumour in a rodent model. The performance of this integrated MR-HIFU system was evaluated in both tissue-mimicking phantoms and rodent studies.

Methods and materials

System description

The hyperthermia system evaluated in this study consisted of multiple hardware and software components described below. Each of these components was tightly integrated and important to achieve precise control of animal body temperature while generating a localised region of heating in a target volume:

1. MRI-compatible preclinical focused ultrasound system (RK100, FUS Instruments, Toronto, Canada): The system was comprised of a 3-axis motorised stage with a single-element focused ultrasound transducer attached to it. The stage enabled precise positioning of the transducer relative to a target region selected from planning MR images. The integrated focused ultrasound transducer had a 75-mm aperture diameter, 60-mm radius of curvature and 56-mm focal length. The operating frequency could be switched between 1.13 MHz and 3.39 MHz (first and third harmonic). The focused ultrasound system and transducer are shown in Figure 1A and B. The system also included the electronics to drive the ultrasound transducer, and software to control positioning and ultrasound transmission. The *in vivo* targeting accuracy of this system was evaluated to be 1.02 ± 0.43 mm in a previous study [44].
2. 3T MR scanner (Ingenia, Philips Healthcare, Amsterdam, Netherlands): The focused ultrasound system was placed inside the MR scanner and images were acquired for treatment planning as well as targeting of the ultrasound beam. In addition, images were acquired continuously during mild hyperthermia treatment to monitor the spatial temperature distribution in the body using the proton resonance frequency (PRF) shift technique for MR thermometry [45,46].
3. Custom-made receive surface coil (Clinical MR Solutions, Brookfield, WI, USA): The surface coil was a single-loop receive coil with a water-proof 3D-printed case which enabled it to be placed under the animal in the fluid path of the beam. This

placement of the coil provided a high signal-to-noise ratio since the coil was directly under the region being heated in the animals. The temperature uncertainty of this coil was calibrated by measuring the standard deviation within an unheated region in a phantom test.

4. Custom-made warming tray: The warming tray was placed over the coil and was comprised of an integrated fluid circuit through which temperature-controlled water could be circulated from a programmable heating/chilling unit (Accel 500LC, Thermo Fisher Scientific, Waltham, MA, USA) located outside the MR console. This tray was very important in achieving and maintaining a stable body temperature in the animals, especially in the MRI environment where experiments could last many hours. Based on our experience, animals often started on the tray slightly warm after preparation in an adjacent workspace, and some cooling (using the tray and the fan on the MRI system) was necessary to bring their temperature to the desired 37 °C. As the experiments progressed, often body temperature would slowly drop and fine adjustments of the temperature of the warming tray enabled us to maintain their core temperature in the desired range. The warming tray had a central opening covered with a thin polyimide film. The target tissue of the animal was placed on the film to enable transmission of ultrasound energy into the body. By using this film on the tray, the animal could be translated or rotated to position the target tissue region over the ultrasound beam without having to manipulate the animal itself. While simple in design, this device enabled efficient positioning of the target tissue volume and maintained stable core temperatures throughout hyperthermia experiments. The warming tray is shown in Figure 1C.
5. 3D-printed acoustic lenses: Sector-vortex lenses were produced with a 3D printer in order to convert the single focus of the transducer into an annulus with a larger overall diameter. More details about the lenses and their characterisation are provided below. A photo of an acoustic lens placed on a transducer is shown in Figure 1B.
6. Real-time software interface: A software interface based on the matMRI library [47] was written in MATLAB which fetched images from the MRI during imaging and calculated the temperature distribution. The software also enabled selection of a region of interest (ROI) for heating and monitoring within the animal, and could utilise these measured temperatures in a feedback control loop to maintain a fixed target temperature.

Sector-vortex lens

Sector-vortex lens design—The traditional sector-vortex lens geometry is designed as a series of wedge-shaped elements arranged as a radial array centred about the central axis of the transducer [48,49]. In this study, a lens was designed to be attached to the front surface of the transducer. By adjusting the thickness of the lens segments, multiple sectors can be created with a phase shift of π between each sector. The number of complete 2π phase rotations about the transducer is referred to as the ‘mode’. Prototype lenses were designed using Solidworks (Waltham) and produced with a 3D printer (Material: Visijet Crystal,

Printer: ProJet 3510 HD Plus, 3D Systems, Rock Hill, SC). The thickness of the lens sectors was determined by the following equation:

$$\left(\frac{D}{v_w} - \frac{D}{v_p}\right) \times 2\pi f = \pi \quad (1)$$

where D is the thickness of lens sector (m), v_w and v_p are the speed of sound in water (m/s) and in the printing material respectively, f is the operating frequency (Hz). v_p was measured to be 2421.5 ± 48.5 m/s, using an acoustic hydrophone and a substitution technique, and v_w was assigned to be 1480 m/s. For a specific printing material, the thickness of the lens was dependent on the operating frequency. After calculating the desired thickness, the lenses were built into three different modes: 4, 8 and 16, creating 8, 16 and 32 heating lobes around the centre, respectively, with progressively increasing diameter.

Acoustic field characterisation

The acoustic intensity distribution produced by different sector-vortex lenses was measured using a needle hydrophone (40 μm active area, SN2188, Precision Acoustics, Dorchester, UK) attached to a three-axis motorised stage (BiSlide, Velmex, Bloomfield, NY) in a degassed water-filled tank [50]. A focused ultrasound transducer with a 75-mm aperture diameter and a 60-mm radius of curvature was placed in the tank with different sector-vortex lenses over the front face. The intensity distribution was measured using the needle hydrophone in two planes – one perpendicular to the face (providing an axial distribution), and one parallel to the face at the focal depth (providing a transverse distribution). The intensity distribution was measured for the first (1.13 MHz), third (3.39 MHz) and fifth (5.63 MHz) harmonic, for each of the three sector-vortex lenses. For all measurements, the focused ultrasound transducer was driven at a 1 kHz repetition frequency with a 20-cycle tone burst using an arbitrary waveform generator (33250A, Agilent Technologies, Santa Clara, CA) and a 42-dB RF amplifier (NP-2947, NP Technologies, Newbury Park, CA). From these measurements, the shape and dimension of the spatial intensity distribution for different operating frequencies and lenses was investigated.

Control software

The control software developed for this system was comprised of three modules: image acquisition, temperature map reconstruction, and temperature control. Magnitude and phase images were acquired and transferred from the MR scanner to the control software via Ethernet utilising a real-time transfer library: matMRI [47]. The transferred phase images were used to calculate temperature maps with the PRF shift method of MR thermometry. In order to achieve an accurate temperature measurement, a 3D second-order iterative drift correction was applied to compensate for magnetic field drift during the duration of imaging, similar to the methods described by Grissom et al. [51,52].

The control algorithm used in this system was a hybrid version of bang-bang [24] and conventional proportional, integral and derivative (PID) controller. The output power can be illustrated with the following equation:

$$P_{out}=\begin{cases} P_{max}, & if\, T \le T_1 \\ K_p e(t)+K_i \int_0^t e(\tau)d\tau+K_d \frac{d}{dt}e(t) \le P_{max}, & if\, T_1<T<T_2 \\ 0, & if\, T_2 \le T \end{cases} \quad (2)$$

where K_p is the proportional gain, K_i is the integral gain, and K_d is the divative gain. These three parameters were optimised empirically through manual tuning in gel phantom experiments to be 0.8, 0.04 and 1.6 respectively. *e* is the error between the measured temperature and the ideal target temperature. *t* is the instantaneous time and τ is the variable of integration. In this study T_1 was set to be 40 °C and T_2 was 43 °C. The controller was turned on with maximum power when the measured temperature was lower than 40 °C and was turned off when the measured temperature was higher than 43 °C. When the temperature was between these thresholds, the output power was manipulated using the PID controller.

Tissue-mimicking phantom experiments

Preliminary hyperthermia experiments were performed in a cylindrical tissue-mimicking phantom (Zerdine, CIRS, Norfolk, VA) to observe the heating pattern created with different sector-vortex lenses. Experiments were performed with four different transducer configurations: 1) heating with a mode 4 lens at 1.13 MHz, 2) heating with a mode 4 lens at 3.39 MHz, 3) heating with a mode 8 lens at 1.13 MHz; and 4) heating with a mode 8 lens at 3.39 MHz. The phantom was placed on top of the small animal MR-HIFU system (as shown in Figure 1A).

After initial survey and calibration scans, T1-weighted images (T1-FFE sequence, echo time (TE) = 5.1 ms, repetition time (TR) = 30 ms, 128 × 128 matrix, field of view (FOV) = 12.8 × 12.8 cm, voxel size = 1.0 × 1.0 × 1.5 mm) were acquired for treatment planning and ultrasound localisation. MR thermometry was performed using a two slice, spoiled gradient echo sequence (T1-FFE sequence, TE = 10 ms, TR = 20.2 ms, 128 × 128 matrix, FOV = 12.8 × 12.8 cm, voxel size = 1.0 × 1.0 × 1.5 mm, acquisition time = 5 s). One image was acquired along the ultrasound beam, and a second transverse to the beam at the focal depth. These images were acquired continuously for 40 min (30 min hyperthermia at 42 °C, 10 min cooling). The acquired MR images were transferred to the control software on the MR-HIFU system and used to calculate the temperature maps. A circular ROI on the transverse temperature map was used as the input to the feedback control algorithm to maintain the target temperature within this region. The diameter of the circular was chosen to match the diameter of the 42 °C isotherm during heating. The ROI was a 5-mm diameter circle for the mode 4 lens, and an 8-mm diameter circle for the mode 8 lens. The maximum output power was 7W (electric) due to the reduced transmission of sound through the plastic.

In vivo experiments

Heating experiments were performed in a rat model (Sprague Dawley, male, *n* = 9, 400–600 g) to evaluate the ability to generate hyperthermia *in vivo*. These experiments were approved by the University of Texas Southwestern Medical Center's Institutional Animal Care and Use Committee. Animals were anaesthetised with a mixture of 2–3% isoflurane and 1–2

L/min of 100% oxygen. A pulse oximeter was attached to the animal's paw to monitor heart rate and oxygen saturation, and a fibre-optic temperature probe was inserted into the rectum to monitor and record core temperature (T1, Neoptix, Canada). Fur covering the animal's thigh was removed using an electric trimmer and depilatory cream (VEET sensitive formula, Parsippany, NJ) to enable transmission of ultrasound into the thigh muscle. The animal was stabilised on the small animal MR-HIFU system, above the warming tray, with the depilated thigh facing the transducer. Ultrasound gel was applied for coupling. The temperature of the warming plate was adjusted until the core temperature of the rat reached a stable temperature of 37 °C.

One group of animals (n = 3) was heated using a bare transducer driven at 1.13 MHz with a maximum electric power of 5W. The other group (n = 6) was heated with a mode 4 lens equipped on the transducer, driven at 3.39 MHz and maximum electric power of 7W. The goal of the two groups was to evaluate the volume of tissue heated with each transducer design. The target temperature in the thigh was 42 °C and the duration of hyperthermia was 30 min.

T1-weighted survey scans (T1-FFE sequence, TE = 5.1 ms, TR = 30 ms, 128 × 128 matrix, FOV = 12.8 × 12.8 cm, voxel size = 1.0 × 1.0 × 1.5 mm) were acquired for treatment planning and localisation of the ultrasound beam (Figure 5A). A preliminary test shot was performed and the region of heating was evaluated in the thigh to ensure the ultrasound beam was not hitting any bones or nerves, to avoid undesirable hot spots or unexpected motion during hyperthermia. After confirmation, a temperature mapping sequence identical to that used for the tissue-mimicking phantom experiment was acquired continuously throughout the entire 30 min of heating and for 10 additional min of cooling. A circular ROI (4-mm diameter circle for the bare transducer group, 5-mm diameter circle for the mode 4 lens group) was used on the transverse temperature maps as input to a feedback control algorithm to control the power delivered to the transducer.

Results

Acoustic field characterisation

Figure 2 shows the normalised transverse spatial intensity distributions for a focused ultrasound transducer paired with different lenses. The columns represent mode 4, 8 and 16 lens, and rows 2–4 represent multiple frequencies: 1.13 MHz, 3.39 MHz and 5.63 MHz (first, third, and fifth harmonics). The first row illustrates the shape and geometry of each lens. For each lens, 8, 16 and 32 heating lobes were present in a circular pattern, with the diameter of the circular region increasing with the mode of the lens. Figure 3 shows the normalised spatial intensity distribution along the ultrasound beam for a focused ultrasound transducer paired with a mode 4 lens at 1.13, 3.39 and 5.63 MHz. Both the lateral and axial extent of the spatial intensity distribution became smaller with higher frequency.

Heating in tissue-mimicking phantom

Figure 4 shows the spatial heating patterns produced in a tissue-mimicking phantom measured with the PRF shift method of MR thermometry. The temperature maps displayed

in the figure are from a single time point after a steady-state temperature of 42 °C was achieved in the phantom. The images were acquired at the focus, both transverse to and along the ultrasound beam. The black contour in each panel indicates a 42 °C isotherm. At 1.13 MHz, a mode 4 lens was able to produce a 4 × 6 mm (diameter × length) heated region, and a mode 8 lens was able to produce a 10 × 12 mm heated region. At 3.39 MHz, a mode 4 lens produced a 2 × 5 mm heated region, while a mode 8 lens produced a 5 × 6 mm heated region. These values were acquired at 10 min as well, when the temperature was maintained stable during the treatment.

In vivo experiments

Figures 5A and D show the treatment planning images with the location of the target region as well as the path of the ultrasound beam in an *in vivo* experiment. The heating pattern produced transverse to the ultrasound beam is shown for the bare transducer operating at 1.13 MHz (Figure 5B) and a mode 4 lens operating at 3.39 MHz (Figure 5C). The heating pattern produced along the ultrasound beam is shown for the bare transducer (E) and the same mode 4 lens (F). Temperature maps were acquired 10 min after the start of mild hyperthermia. The black contour in each panel indicates a 42 °C isotherm. The ability to expand the region of heating with the sector-vortex lens is apparent in the figure. Figure 6 includes temperature maps acquired at different time points (0, 3, 5, 10, 20, 30, 35, 38 and 40 min) to confirm that the heating effect was well-controlled at the target region through the entire 30 min treatment period, without causing undesired heating within the surrounding tissue.

Temperature control

Figure 7 shows the mean temperature within the feedback control ROI in the temperature maps during the phantom (panel A) and animal (panel B) experiments. Three curves are included in each plot: the mean temperature (T mean), the temperature exceeded by 10% of pixels (T10), and the temperature exceeded by 90% of pixels (T90). The output electrical power over the duration of heating is also shown. Excellent control of temperatures was achieved in both the tissue-mimicking phantom and rodent model using this system. A slight overshoot to 43.7 °C (34%) and oscillation in temperatures was observed at the beginning of each treatment due to the bang-bang component of the control algorithm. The temperature reached 42 °C within 3 min and was well-maintained at 42 °C for the desired treatment period (30 min). The output power stabilised at approximately 2.5W during the treatment in the phantom experiment and approximately 3.5W in the animal experiment conducted with a mode 4 lens.

A summary of the temperatures achieved in the *in vivo* experiments is given in Table 1. The mean temperature within the heated ROI was 42.1 ± 0.3 °C, with a T10 and T90 of 43.2 ± 0.4 °C and 41.0 ± 0.3 °C respectively. The time in range was defined as the period when all pixels within the heated ROI were between 41–45 °C. This range was selected so that the heating effect can trigger the rapid release of the thermosensitive liposomes without causing any disruption to the blood flow. In this study, the time in range was estimated to be 31.1 min across nine animals.

Discussion and conclusion

In this study we demonstrated that a preclinical MR-HIFU system can be adapted to perform precisely controlled hyperthermia in tissue-mimicking phantoms and small animals. This approach has the advantages of being non-invasive and able to create localised heating within targets in rodent models. The system described in this study was able to perform localised mild hyperthermia treatment for up to 30 min, although longer durations should be possible. The temperature distribution was well-controlled within the focal region to a defined set point, and different heating patterns were created when paired with 3D printed sector-vortex lenses.

When applying focused ultrasound for hyperthermia, the major limitation of focused ultrasound transducers is the small volume of heating achieved at the focus. Normally electronic or mechanical steering is implemented to distribute the focused ultrasound energy across a larger volume [30,53–57]. In this study we evaluated a 3D printed sector-vortex lens to broaden the acoustic intensity distribution in order to heat a larger tissue volume. Compared to traditional phased array transducers, the 3D printed lenses are simpler and more cost-effective to produce. One set of lenses with different sizes will be able to create various heating patterns without switching the transducer. The utilisation of transducer harmonics added another dimension of control along the length of the transducer to customise the heating region to various sizes of preclinical targets. The major benefits of the plastic lenses are the ability to heat a larger tissue volume without any transducer motion (a common source of artefacts in MR thermometry), and the ability to achieve a complex spatial intensity distribution without the use of a phased array. The disadvantage of these lenses is that they are fixed in geometry so do not allow dynamic adjustment of the spatial energy distribution during heating. However, in these preliminary heating experiments in rodents, this lack of dynamic control did not appear to be a limiting factor in achieving relatively uniform heating regions.

In addition to the transducer, the integration of a custom surface coil and warming tray were essential components of the hyperthermia system. The RF coil enabled acquisition of temperature maps with a 1 × 1 × 1.5 mm voxel size and a temperature uncertainty of less than 0.5 °C, which provided high fidelity measurements for the feedback control algorithm. The warming tray was critical in maintaining the systemic temperature of the rodents at a constant temperature of 37 °C throughout the heating experiment to avoid systemic hypothermia (body temperature below 35 °C) or hyperthermia (body temperature greater than 37.5–38.3 °C). This feature is especially important in the exploration of temperature-sensitive nanoparticles for targeted drug delivery.

The temperature feedback control algorithm utilised with the hyperthermia platform in this study was comprised of an initial bang-bang controller which converted to a conventional PID controller once a threshold temperature was reached. This combination allowed the algorithm to create a relatively fast temperature rise at the beginning, and to maintain the temperature at the target temperature for longer durations. While this was successful overall, the PID tuning parameters were selected using manual tuning with a bare transducer, and it was observed that the parameters were somewhat sensitive to different conditions, especially

when paired with lenses. The temperature drop and oscillation observed at the beginning of each treatment was caused by the power adjustment that happened when the algorithm switched from bang-bang to regular PID. The output power decreased from P_{max} to about 2W after the switch, resulting in the dip in the temperature observed. Future versions of the controller will implement a proportional logic in the initial heating phase to achieve a smoother temperature transition from the initial rise to the steady-state phase, and to compensate better for different lenses. While PID tuning parameters must be selected manually for different transducers and anatomical targets, this framework allowed for accurate and repeatable temperature control for hyperthermia in rat thigh with the transducers and lenses described in this study.

Finally, the targets selected for heating in the initial *in vivo* experiments were all within the rat thigh. This represented a target similar to what one would expect with an implanted subcutaneous or intramuscular tumour. However, for orthotropic tumours in the liver, prostate, or other organs that requires discrete control of hyperthermia, a customised transducer design and motion-compensated temperature control algorithm may be necessary. These will be the subject of future investigations as the need arises.

Acknowledgments

Financial support for this study was provided by the Cancer Prevention and Research Initiative of Texas, grant nos. R1308, 1R01CA199037-01 and generous donation from the M.R. and Evelyn Hudson Foundation. R.S. is an employee of Philips Research. R.C. is a co-founder of FUS Instruments, the company that manufactured the preclinical focused ultrasound system that was adapted in this study for hyperthermia exposures. The company provided no financial support for this study. The authors alone are responsible for the content and writing of the paper.

References

1. Baronzio G. A brief overview of hyperthermia in cancer treatment. J Integr Oncol. 2014; 03:1–10.
2. Baronzio, G.; Hager, E. Hyperthermia in cancer treatment: A primer. New York: Springer; 2006. Available from: http://scholar.google.com/scholar?hl=en&btnG=Search&q=intitle:Hyperthermia+in+cancer+Treatment:+A+primer#0\nhttp://scholar.google.com/scholar?hl=en&btnG=Search&q=intitle:Hyperthermia+in+cancer+treatment:+a+primer#0\nhttp://www.landesbioscience.com/iu/Baro.
3. Hurwitz MD, Hansen JL, Prokopios-Davos S, Manola J, Wang Q, Bornstein BA, et al. Hyperthermia combined with radiation for the treatment of locally advanced prostate cancer: Long-term results from Dana-Farber Cancer Institute study 94-153. Cancer. 2011; 117:510–516. [PubMed: 20886629]
4. Jones EL, Oleson JR, Prosnitz LR, Samulski TV, Vujaskovic Z, Yu D, et al. Randomized trial of hyperthermia and radiation for superficial tumors. J Clin Oncol. 2005; 23:3079–3085. [PubMed: 15860867]
5. De Bruijne M, Van der Zee J, Ameziane A, Van Rhoon GC. Quality control of superficial hyperthermia by treatment evaluation. Int J Hyperthermia. 2011; 27:199–213. [PubMed: 21501023]
6. Gellermann J, Hildebrandt B, Issels R, Ganter H, Wlodarczyk W, Budach V, et al. Noninvasive magnetic resonance thermography of soft tissue sarcomas during regional hyperthermia: Correlation with response and direct thermometry. Cancer. 2006; 107:1373–1382. [PubMed: 16902986]
7. Hall EJ, Roizin-Towle L. Biological effects of heat. Caner Res. 1984; 44(Suppl10):S4708–S4713.
8. Dewey WC. Arrhenius relationships from the molecule and cell to the clinic. Int J Hyperthermia. 2009; 25:3–20. [PubMed: 19219695]

9. Hurwitz MD. Today's thermal therapy: Not your father's hyperthermia: Challenges and opportunities in application of hyperthermia for the 21st century cancer patient. Am J Clin Oncol. 2010; 33:96–100. [PubMed: 19636240]
10. Xu Y, Choi J, Hylander B, Sen A, Evans SS, Kraybill WG, et al. Fever-range whole body hyperthermia increases the number of perfused tumor blood vessels and therapeutic efficacy of liposomally encapsulated doxorubicin. Int J Hyperthermia. 2007; 23:513–527. [PubMed: 17952765]
11. Bleehen NM, Honess DJ, Morgan JE. Interaction of hyperthermia and the hypoxic cell sensitizer Ro-07-0582 on the EMT6 mouse tumour. Br J Cancer. 1977; 35:299–306. [PubMed: 856237]
12. Imamura M, Seki T, Tamai T, Kunieda K, Nakatani S, Yamashiki N, et al. Change of temperature in mouse tumour tissue immersed in a water bath at 44 °C. Oncol Rep. 1998; 5:1061–1064. [PubMed: 9683808]
13. Locke J, Zeug A, Thompson DJ, Allan J, Mazzarella K, Novak P, et al. Localized versus regional hyperthermia: Comparison of xenotransplants treated with a small animal ultrasound system and waterbath limb immersion. Int J Hyperthermia. 2005; 21:271–281. [PubMed: 16019853]
14. Robinson JE, Harrison GH, McCready WA, Samaras GM. Good thermal dosimetry is essential to good hyperthermia research. Br J Radiol. 2014; 41(607):651.10.1259/0007-1285-51-607-532
15. Giovanella BC, Stehlin JS, Shepard RC, Williams LJ. Hyperthermic treatment of human tumors heterotransplanted in nude mice. Cancer Res. 1979; 39:2236–2241. [PubMed: 445423]
16. Vojnovic B, Joiner MC. A multiple RF heating system for experimental hyperthermia in small animals. Int J Hyperthermia. 1985; 1:287–298. [PubMed: 3836274]
17. Bolmsjo M, Hafstrom L, Hugander A, Jonsson PE, Persson B. Experimental set-up for studies of microwave-induced hyperthermia in rats. Phys Med Biol. 1982; 27:397–406. [PubMed: 7071151]
18. Gottlieb CF, Block NL. A technique for localized tumor hyperthermia in small animals. Med Instrum. 1987; 21:75–80. [PubMed: 3614034]
19. Bruggmoser G, Hinkelbein W, Saum R. Experimental thermo-radiotherapy of human tumour xenografts in nude mice; design of the hyperthermia system. Int J Hyperthermia. 1992; 8:631–643. [PubMed: 1402140]
20. Huang SK, Stauffer PR, Hong K, Guo JWH, Phillips TL, Huang A, et al. Liposomes and hyperthermia in mice: Increased tumor uptake and therapeutic efficacy of doxorubicin in sterically stabilized liposomes. Cancer Res. 1994; 54:2186–2191. [PubMed: 8174126]
21. Kaatee RS, Kampmeijer AG, van Hooije CM, van Rhoon GC, Kanis AP, Levendag PC, et al. A 27 MHz current source interstitial hyperthermia system for small animals. Int J Hyperthermia. 1995; 11:785–796. [PubMed: 8586900]
22. Attaluri A, Ma R, Qiu Y, Li W, Zhu L. Nanoparticle distribution and temperature elevations in prostatic tumours in mice during magnetic nanoparticle hyperthermia. Int J Hyperthermia. 2011; 27:491–502. [PubMed: 21756046]
23. Ebbini ES, Cain CA. Multiple-focus ultrasound phased-array pattern synthesis: Optimal driving-signal distributions for hyperthermia. IEEE Trans Ultrason Ferroelectr Freq Control. 1989; 36:540–548. [PubMed: 18290231]
24. Lin WL, Roemer RB, Hynynen K. Theoretical and experimental evaluation of a temperature controller for scanned focused ultrasound hyperthermia. Med Phys Radiat Oncol. 1990; 17:615–625.
25. Daum DR, Smith NB, King R, Hynynen K. In vivo demonstration of noninvasive thermal surgery of the liver and kidney using an ultrasonic phased array. Ultrasound Med Biol. 1999; 25:1087–1098. [PubMed: 10574341]
26. Singh AK, Moros EG, Novak P, Straube W, Zeug A, Locke JE, et al. MicroPET-compatible, small animal hyperthermia ultrasound system (SAHUS) for sustainable, collimated and controlled hyperthermia of subcutaneously implanted tumours. Int J Hyperthermia. 2004; 20:32–44. [PubMed: 14612312]
27. Sun L, Collins CM, Schiano JL, Smith MB, Smith NB. Adaptive real-time closed-loop temperature control for ultrasound hyperthermia using magnetic resonance thermometry. Concepts Magn Reson Part B. 2005; 27:51–63.

28. Chopra R, Curiel L, Staruch R, Morrison L, Hynynen K. An MRI-compatible system for focused ultrasound experiments in small animal models. Med Phys Imaging Res. 2009; 36:1867–1874.
29. Staruch R, Chopra R, Hynynen K. Localised drug release using MRI-controlled focused ultrasound hyperthermia. Int J Hyperthermia. 2011; 27:156–171. [PubMed: 21158487]
30. Hijnen NM, Heijman E, Kohler MO, Ylihautala M, Ehnholm GJ, Simonetti AW, et al. Tumour hyperthermia and ablation in rats using a clinical MR-HIFU system equipped with a dedicated small animal set-up. Int J Hyperthermia. 2012; 28:141–155. [PubMed: 22335228]
31. Partanen A, Yarmolenko PS, Viitala A, Appanaboyina S, Haemmerich D, Ranjan A, et al. Mild hyperthermia with magnetic resonance-guided high-intensity focused ultrasound for applications in drug delivery. Int J Hyperthermia. 2012; 28:320–336. [PubMed: 22621734]
32. Ernsting MJ, Worthington A, May JP, Tagami T, Kolios MC, Li SD. Ultrasound drug targeting to tumors with thermosensitive liposomes. Proc IEEE Int Ultrason Symp. 2011:1–4.
33. Fite BZ, Liu Y, Kruse DE, Caskey CF, Walton JH, Lai CY, et al. Magnetic resonance thermometry at 7T for real-time monitoring and correction of ultrasound induced mild hyperthermia. PLoS One. 2012; 7:7. (4). 10.1371/journal.pone.0035509
34. Salomir R, Vimeux FC, de Zwart JA, Grenier N, Moonen CT. Hyperthermia by MR-guided focused ultrasound: Accurate temperature control based on fast MRI and a physical model of local energy deposition and heat conduction. Magn Reson Med. 2000; 43:342–347. [PubMed: 10725875]
35. Mougenot C, Salomir R, Palussière J, Grenier N, Moonen CTW. Automatic spatial and temporal temperature control for MR-guided focused ultrasound using fast 3D MR thermometry and multispiral trajectory of the focal point. Magn Reson Med. 2004; 52:1005–1015. [PubMed: 15508173]
36. Hijnen NM, Heijman E, Köhler MO, Ylihautala M, Ehnholm GJ, Simonetti AW, et al. Tumour hyperthermia and ablation in rats using a clinical MR-HIFU system equipped with a dedicated small animal set-up. Int J Hyperthermia. 2012; 28:141–155. [PubMed: 22335228]
37. De Smet M, Heijman E, Langereis S, Hijnen NM, Grüll H. Magnetic resonance imaging of high intensity focused ultrasound mediated drug delivery from temperature-sensitive liposomes: An in vivo proof-of-concept study. J Control Release. 2011; 150:102–110. [PubMed: 21059375]
38. Kazanzides P, Chang J, Iordachita I, Li J, Ling CC, Fichtinger G. Design and validation of an image-guided robot for small animal research. Med Image Comput Comput Interv. 2006; 9:50–57.
39. Sasaki K, Medan MS, Azuma T, Kawabata K, Shimoda M, Umemura S. Effect of echo-guided high-intensity focused ultrasound ablation on localized experimental tumors. J Vet Med Sci. 2006; 68:1069–1074. [PubMed: 17085885]
40. Staruch R, Chopra R, Hynynen K. Hyperthermia in bone generated with MR imaging-controlled focused ultrasound: Control strategies and drug delivery. Radiology. 2012; 263:117–127. [PubMed: 22438444]
41. Nance E, Timbie K, Miller GW, Song J, Louttit C, Klibanov AL, et al. Non-invasive delivery of stealth, brain-penetrating nanoparticles across the blood–brain barrier using MRI-guided focused ultrasound. J Control Release. 2014; 189:123–132. [PubMed: 24979210]
42. Oakden W, Kwiecien JM, O'Reilly MA, Lake EMR, Akens MK, Aubert I, et al. A non-surgical model of cervical spinal cord injury induced with focused ultrasound and microbubbles. J Neurosci Methods. 2014; 235:92–100. [PubMed: 24970578]
43. Huang Y, Vykhodtseva NI, Hynynen K. Creating brain lesions with low-intensity focused ultrasound with microbubbles: A rat study at half a megahertz. Ultrasound Med Biol. 2013; 39:1420–1428. [PubMed: 23743099]
44. Ellens NPK, Kobelevskiy I, Chau A, Waspe AC, Staruch RM, Chopra R, et al. The targeting accuracy of a preclinical MRI-guided focused ultrasound system. Med Phys. 2015; 42:430–439. [PubMed: 25563283]
45. Ishihara Y, Calderon A, Watanabe H, Okamoto K, Suzuki Y, Kuroda K, et al. A precise and fast temperature mapping using water proton chemical shift. Magn Reson Med. 1995; 34:814–823. [PubMed: 8598808]

46. McDannold N. Quantitative MRI-based temperature mapping based on the proton resonant frequency shift: Review of validation studies. Int J Hyperthermia. 2005; 21:533–546. [PubMed: 16147438]
47. Zaporzan B, Waspe A, Looi T, Mougenot C, Partanen A, Pichardo S. MatMRI and MatHIFU: Software toolboxes for real-time monitoring and control of MR-guided HIFU. J Ther Ultrasound. 2013; 1:7. [PubMed: 25512856]
48. Fjield T, Sorrentino V, Cline H, Hynynen K. Design and experimental verification of thin acoustic lenses for the coagulation of large tissue volumes. Phys Med Biol. 1997; 42:2341–2354. [PubMed: 9434292]
49. Umemura S, Cain CA. The sector-vortex array: Acoustic field synthesis for hyperthermia. IEEE Trans Ultrason Ferroelect Freq Contr. 1989; 36:249–257.
50. Bing C, Ladouceur-Wodzak M, Wanner CR, Shelton JM, Richardson JA, Chopra R. Trans-cranial opening of the blood–brain barrier in targeted regions using a stereotaxic brain atlas and focused ultrasound energy. J Ther Ultrasound. 2014; 2:13. [PubMed: 25232482]
51. Grissom WA, Rieke V, Holbrook AB, Medan Y, Lustig M, Santos J, et al. Hybrid referenceless and multibaseline subtraction MR thermometry for monitoring thermal therapies in moving organs. Med Phys. 2010; 37:5014–5026. [PubMed: 20964221]
52. Grissom WA, Lustig M, Holbrook AB, Rieke V, Pauly JM, Butts-Pauly K. Reweightedl1 referenceless PRF shift thermometry. Magn Reson Med. 2010; 64:1068–1077. [PubMed: 20564600]
53. Lu M, Wan M, Xu F, Wang X, Chang X. Design and experiment of 256-element ultrasound phased array for noninvasive focused ultrasound surgery. Ultrasonics. 2006; 44:e325–e330. [PubMed: 16949119]
54. Gateau J, Marsac L, Pernot M, Aubry JF, Tanter M, Fink M. Transcranial ultrasonic therapy based on time reversal of acoustically induced cavitation bubble signature. IEEE Trans Biomed Eng. 2010; 57:134–144. [PubMed: 19770084]
55. Staruch RM, Hynynen K, Chopra R. Hyperthermia-mediated doxorubicin release from thermosensitive liposomes using MR-HIFU: Therapeutic effect in rabbit Vx2 tumours. Int J Hyperthermia. 2015; 31:118–133. [PubMed: 25582131]
56. Yarmolenko PS, Gallardo ENC, Partanen A, Ranjan A, Burke C, Bartels LW, et al. Large volume, conformal hyperthermia with magnetic resonance-guided high intensity focused ultrasound. Proc Soc Therm Med. 2012; 19
57. Salomir R, Delemazure AS, Palussiere J, Rouviere O, Cotton F, Chapelon JY. Image-based control of the magnetic resonance imaging-guided focused ultrasound thermotherapy. Top Magn Reson Imaging. 2006; 17:139–151. [PubMed: 17414071]

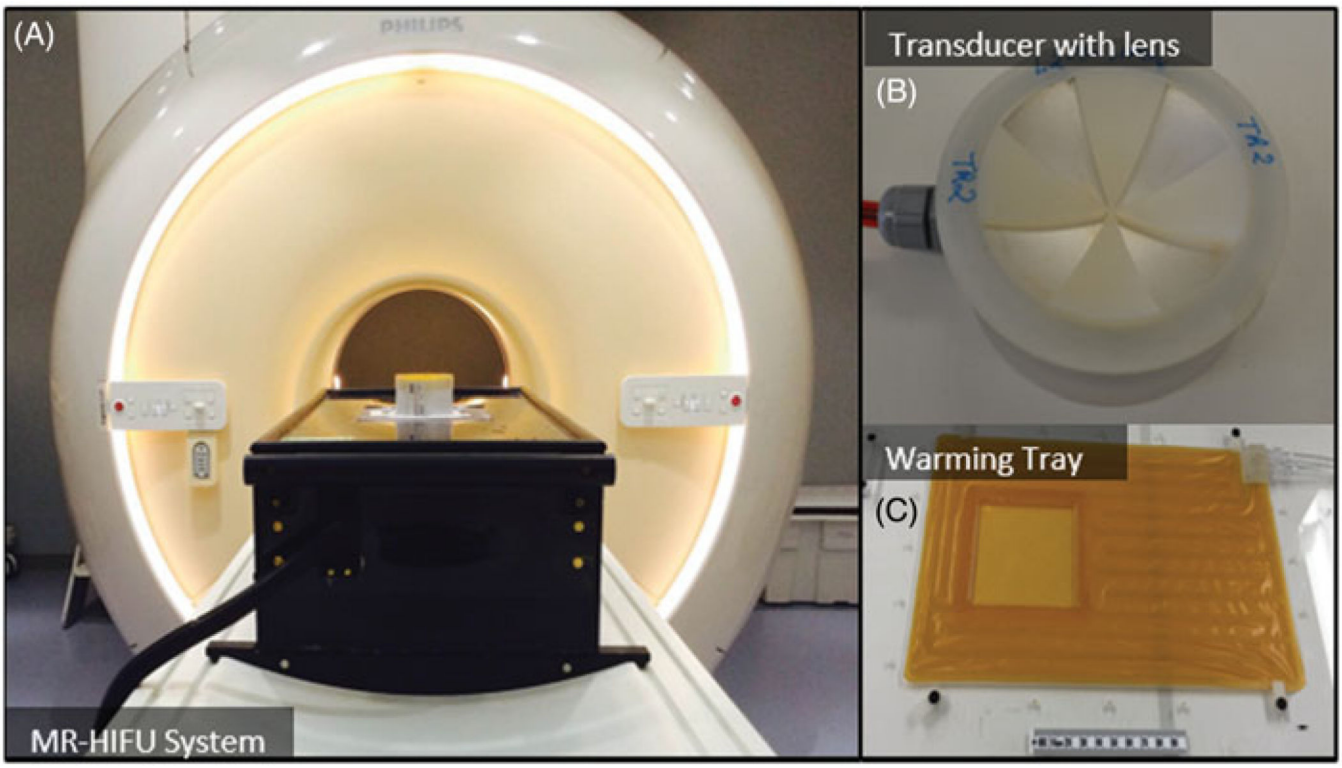

Figure 1.
Components of an MRI-compatible focused ultrasound system used to generate hyperthermia exposures in preclinical experiments. A) The MRI-compatible positioning system is positioned on the patient table of a clinical MR scanner. B) A focused transducer with a 3D-printed acoustic lens. C) Warming tray used to maintain the body temperature of the animal.

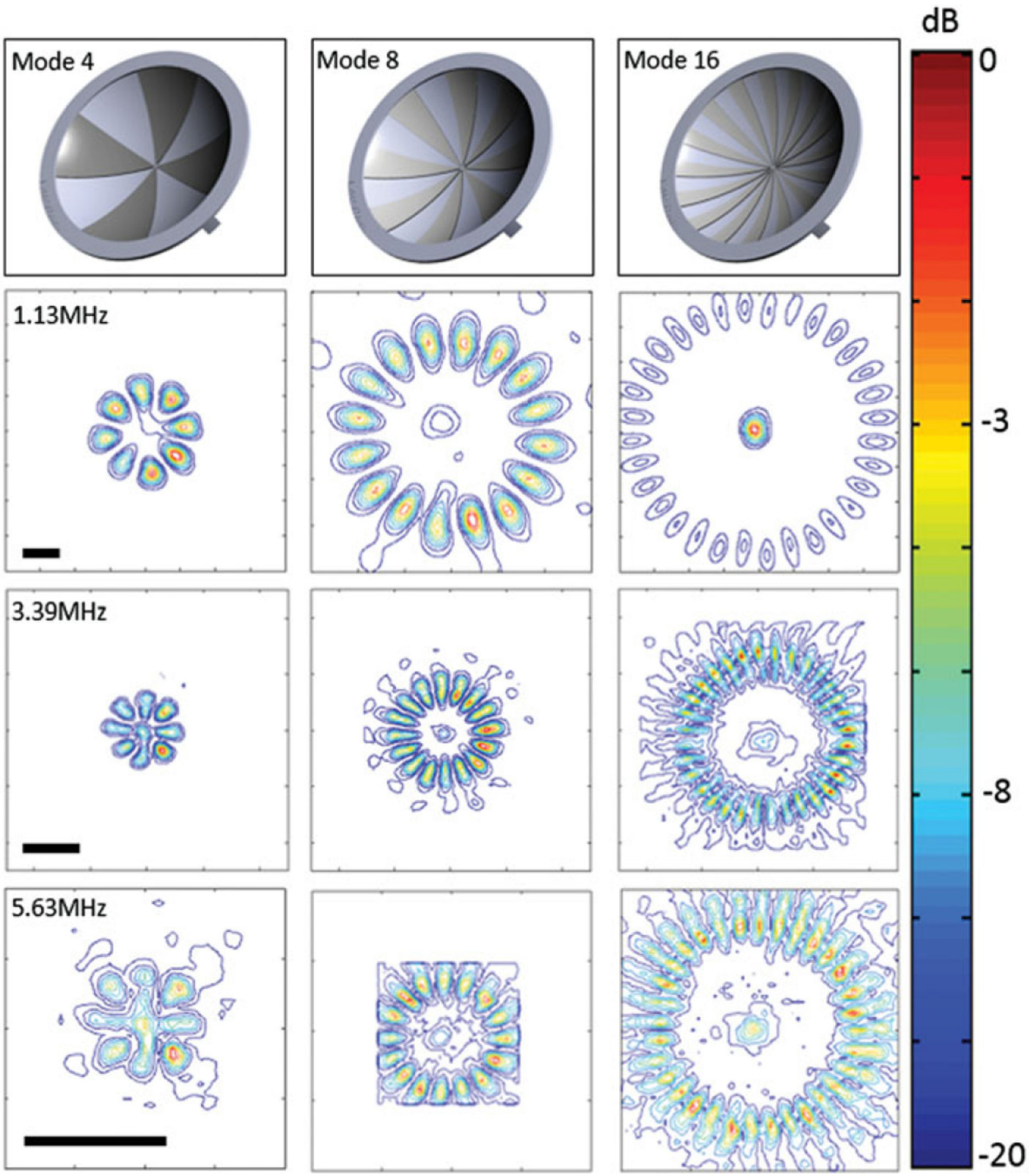

Figure 2.

Sector-vortex lens design and normalised contour plots of the spatial intensity distribution parallel to the face of the transducer, at the focal depth (scale bar 2 mm). The location of the focal region remained relatively constant for the different mode lenses.

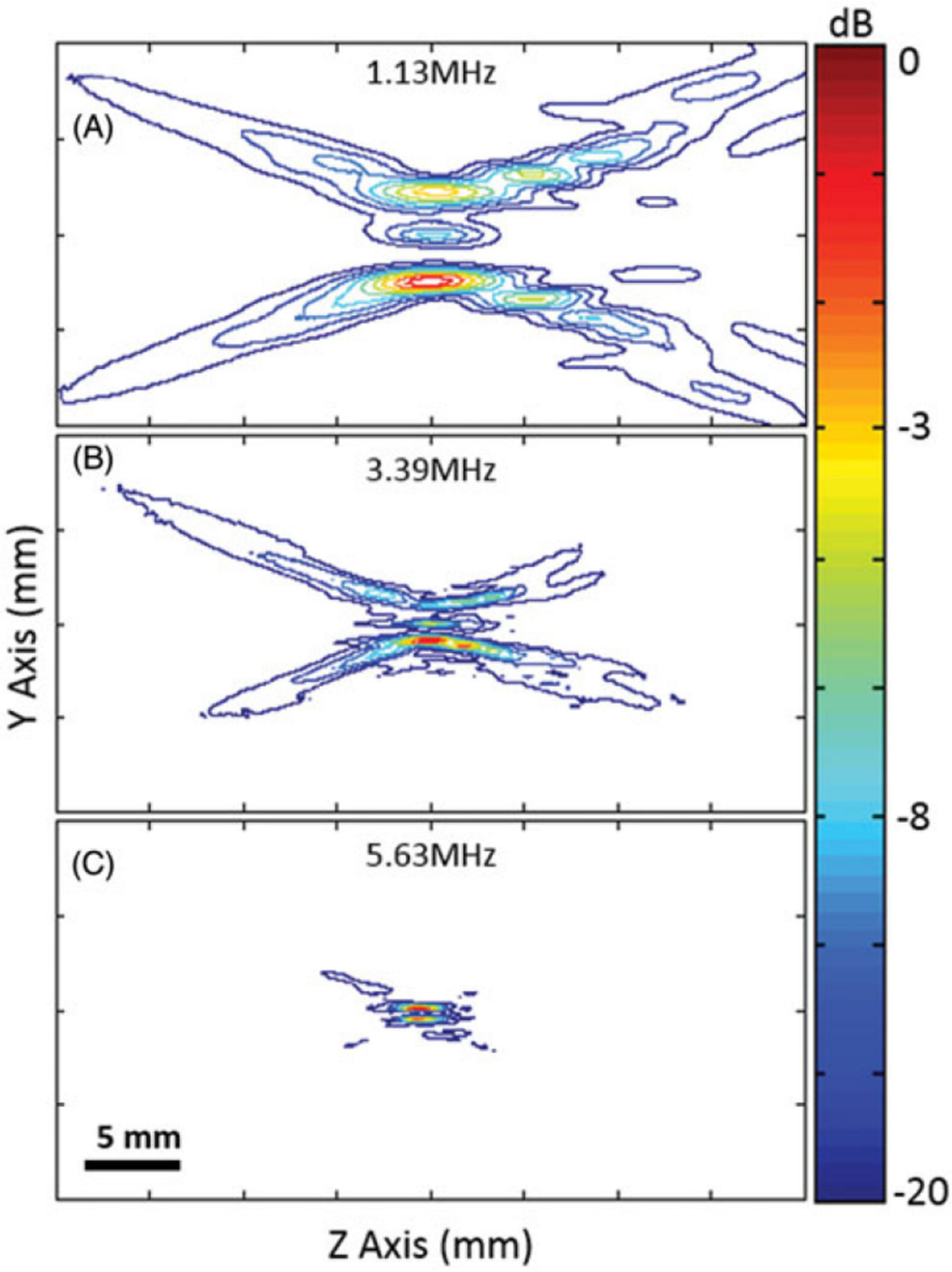

Figure 3.
Normalised contour plots of the spatial intensity distribution along the ultrasound beam axis at three different frequencies, using a mode 4 lens.

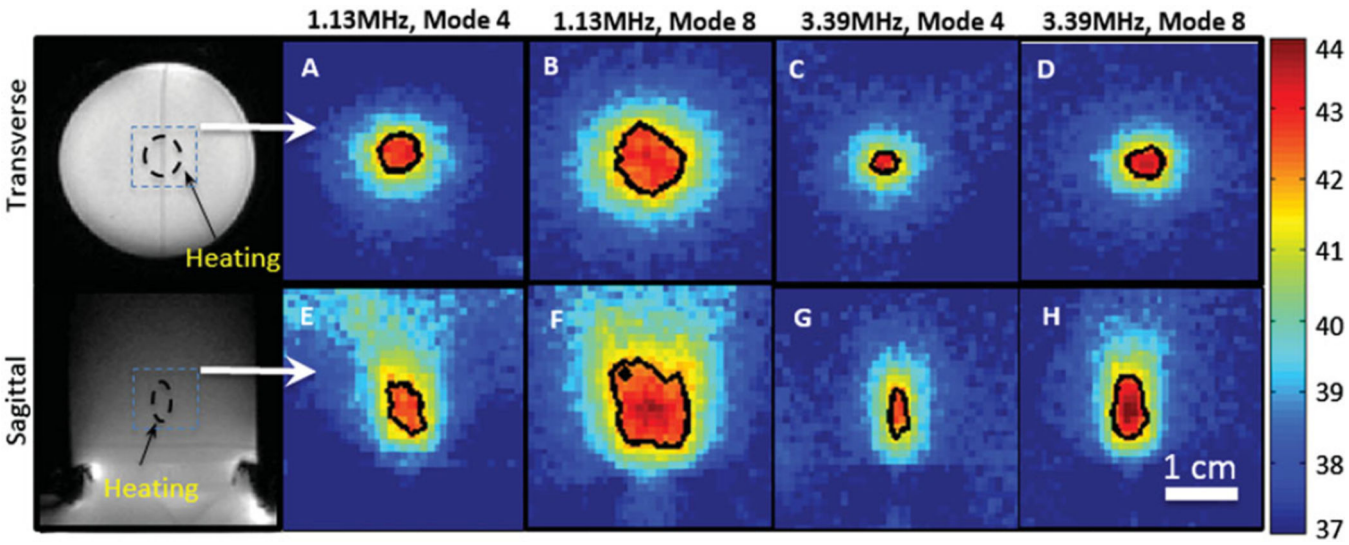

Figure 4.

Spatial heating patterns produced in a tissue-mimicking phantom using different combinations of frequencies and lenses. The black contour in each panel indicates the 42 °C isotherm. The temperature distributions transverse (A–D) and along (E–H) the ultrasound beam axis are shown. The location of heating in the phantom is shown in the magnitude images.

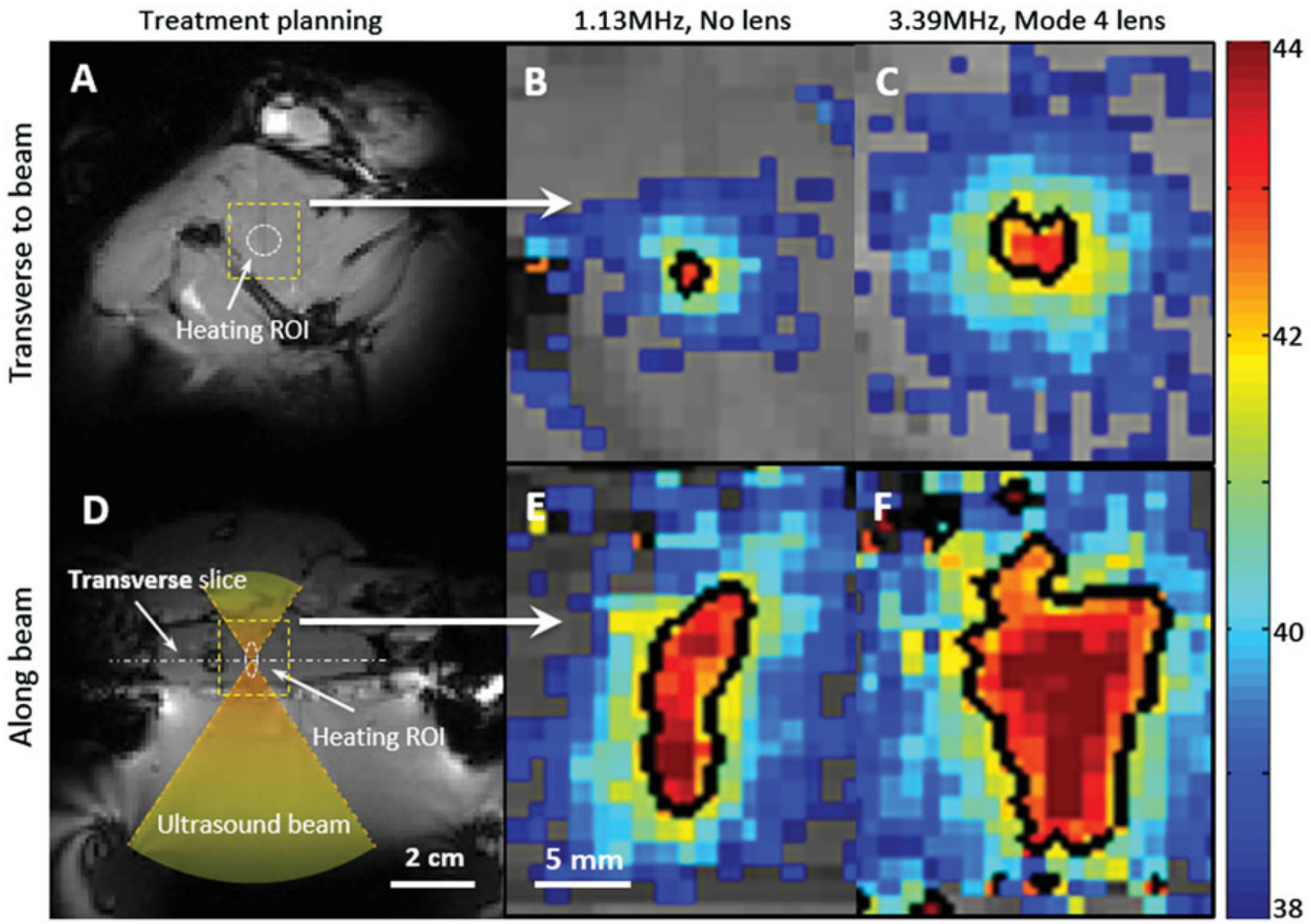

Figure 5.

Zoomed-in spatial heating patterns(within the dotted boxes in A, D) measured in a rat thigh with a bare transducer operating at 1.13 MHz (B, E) or a mode 4 lens operating at 3.39 MHz (C, F). The temperature maps were acquired at 10 min after sonication. The top panels show the heating transverse to the beam in the focal plane, and the bottom panels show the heating along the beam. Panels A and D depict the process of treatment planning and the location of heating ROI. The black contour indicates the 42 °C isotherm.

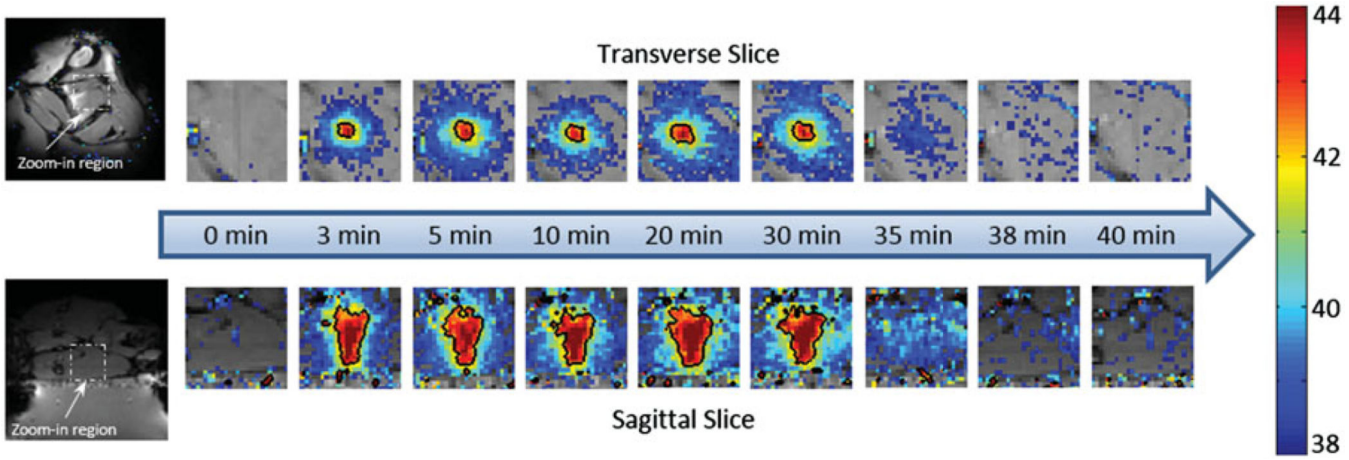

Figure 6.

The temperature maps acquired at different time points during the *in vivo* experiment. Nine time points were selected to represent pre-treatment, during treatment and post-treatment, separately. The black contour showed the 42 °C isotherm. Uniform heating pattern was observed during the treatment. Post-treatment maps indicated that no undesired heating was created within the surrounding tissue.

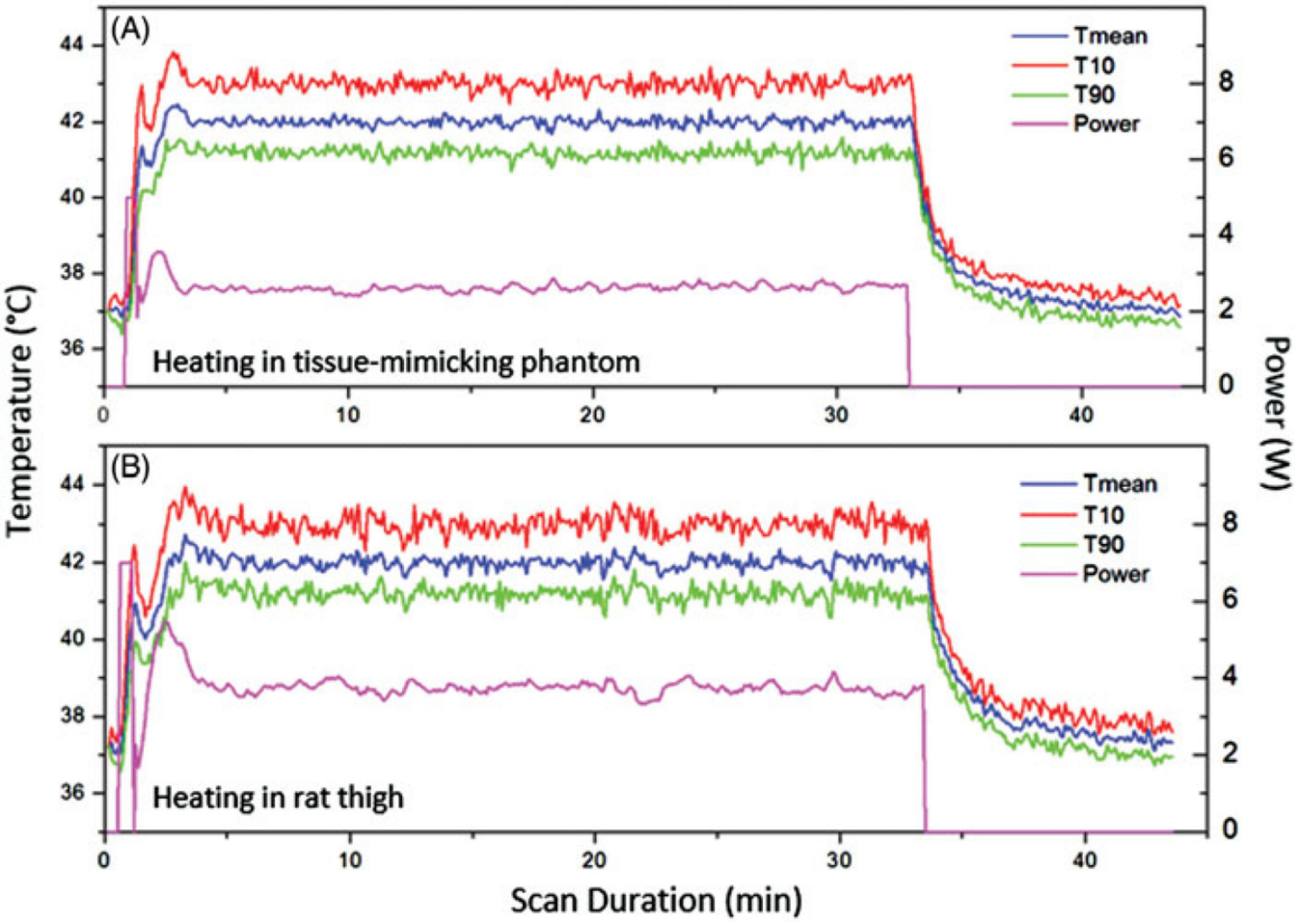

Figure 7.

The mean, 10th and 90th percentile temperatures versus time in a central ROI within a tissue-mimicking phantom (A) and rat thigh (B). The output power versus time is also shown for each experiment. Very stable heating was achieved throughout the hyperthermia experiment.

Table 1

Heating performance across nine animals.

Experiment ID	Tmean (°C)	T10 (°C)	T90 (°C)	Body temp (°C)	Time in range (min)
Rat 1	42.5 ± 0.8	43.7 ± 0.9	41.3 ± 0.7	37.3 ± 0.7	30.1
Rat 2	42.0 ± 0.3	43.5 ± 0.4	40.7 ± 0.3	37.1 ± 0.5	30.9
Rat 3	42.0 ± 0.3	43.1 ± 0.4	41.1 ± 0.3	37.1 ± 1.1	30.7
Rat 4	42.0 ± 0.2	43.0 ± 0.2	41.1 ± 0.2	37.6 ± 1.3	30.4
Rat 5	42.0 ± 0.2	43.3 ± 0.3	41.0 ± 0.3	37.1 ± 0.7	31.8
Rat 6	42.0 ± 0.2	42.7 ± 0.3	41.1 ± 0.3	37.6 ± 0.3	31.7
Rat 7	42.0 ± 0.2	43.7 ± 0.3	40.5 ± 0.3	37.5 ± 0.7	31.3
Rat 8	42.0 ± 0.2	43.0 ± 0.3	41.2 ± 0.2	37.1 ± 0.3	31.4
Rat 9	42.0 ± 0.2	43.2 ± 0.3	40.9 ± 0.2	36.8 ± 1.2	31.5
Average	42.1 ± 0.3	43.2 ± 0.4	41.0 ± 0.3	37.2 ± 0.8	31.1